UNIVERSITY OF LEEDS

This is a repository copy of *Assessment of Cellular Beams with Transverse Stiffeners and Closely Spaced Web Openings*.

White Rose Research Online URL for this paper:
http://eprints.whiterose.ac.uk/85944/

Version: Accepted Version

Article:
Tsavdaridis, KD and Galiatsatos, G (2015) Assessment of Cellular Beams with Transverse Stiffeners and Closely Spaced Web Openings. Thin-Walled Structures, 94. pp. 636-650. ISSN 0263-8231

https://doi.org/10.1016/j.tws.2015.05.005

© 2015, Elsevier. Licensed under the Creative Commons Attribution-NonCommercial-NoDerivatives 4.0 International
http://creativecommons.org/licenses/by-nc-nd/4.0/

Reuse
Unless indicated otherwise, fulltext items are protected by copyright with all rights reserved. The copyright exception in section 29 of the Copyright, Designs and Patents Act 1988 allows the making of a single copy solely for the purpose of non-commercial research or private study within the limits of fair dealing. The publisher or other rights-holder may allow further reproduction and re-use of this version - refer to the White Rose Research Online record for this item. Where records identify the publisher as the copyright holder, users can verify any specific terms of use on the publisher's website.

Takedown
If you consider content in White Rose Research Online to be in breach of UK law, please notify us by emailing eprints@whiterose.ac.uk including the URL of the record and the reason for the withdrawal request.

White Rose university consortium
Universities of Leeds, Sheffield & York

eprints@whiterose.ac.uk
https://eprints.whiterose.ac.uk/

Assessment of Cellular Beams with Transverse Stiffeners and Closely Spaced Web Openings

[1]Konstantinos Daniel Tsavdaridis and [2]Grigorios Galiatsatos

[1]Lecturer in Structural Engineering, School of Civil Engineering, University of Leeds, LS2 9JT, Leeds
[2]Engineer, School of Civil Engineering, University of Leeds, LS2 9JT, Leeds

---

Abstract: A computational parametric finite element analysis was carried out, investigating closely spaced cellular beams with double concentric transverse stiffeners. An unstiffened perforated beam section was initially designed and validated against existing finite element analysis results found in the literature. Then, twenty seven models were studied, while altering the spacing between the web openings, the web thicknesses and the stiffener thicknesses. The results showed that Vierendeel shearing failure occurred more frequently for very closely spaced sections. However, as the spacing increased, the contribution of the stiffener to strength of the section was decreased, and buckling failure occurred more often. A maximum distance for the spacing between the openings was suggested. At last, a design model was proposed, where for very closely spaced openings the compressive stresses were given by the Vierendeel moment capacity, and for the maximum distance of the spacing between the openings studied, the compressive stresses were given by a strut analogy, as found in BS5950–1.

---

1. Introduction

1.1 Perforated Beams

Recently, there has been an increase in the use of perforated beams in steel and composite buildings as well as girders with web openings when used in bridges or as deep transfer beams in the lower floors of high-rise buildings. Beams and girders with web openings trade shear capacity for cost effectiveness and ease of construction of a structure [1].

Primary issues that have arisen with the use of perforated beams relate to the location of openings along the length of the beam, the shape the openings should have, how large the openings should be, and the proximity of the openings to each other [1]. Significant experimental and theoretical research has been made in the last decade [2,3,4,5,6] with the aim to maximize the web opening area and minimize the self-weight of the beam.

1.2 Stiffeners

It is common practice to use stiffeners to strengthen the moment resistance of steel plates and connections along the longitudinal and/or transverse direction when designing lightweight structures. Considerable research, both experimental and theoretical, on transverse stiffeners has been undertaken over the last four decades resulting in several design models [7,8,9,10,11,12,13,14,15]. Eurocode 3 and BS5950–1 base the design of stiffeners on these models. These codes produce slightly different designs however, and so for clarity some of these differences are summarised in **Table 1**.

Examining the aforementioned codes, it is observed that there is no knowledge of how a beam with web openings would behave if a transverse stiffener was placed between two adjacent web openings. A computational Finite Element (FE) analysis and a parametric study of a transversely stiffened perforated beam with web openings, aims to achieve a full understanding of its behaviour, allowing for an update to the current approximation.

2. Model Validation

The validation of the FE model, presented by Tsavdaridis and D'Mello [5], was conducted in ANSYS Multiphysics v11.0. A UKB section of $457\ x\ 152\ x\ 52$ was selected.

Standard	EC3	BS5950–1
Tension Field Action	Exact angle of inclination of tension field, shear capacity is maximised	Tension field depends on the flange section, more conservative value for shear capacity
Design for Shear Buckling with Stiffeners	Restriction of aspect to panel ratio between 1.0 and 3.0	No restrictions of aspect to panel ratio
Flange Buckling	Does not include effect of web stiffeners, includes guidance for curved members	Includes effect of web stiffeners, but no guidance for curved members
Design for Serviceability	Not covered	Minimum web thickness value
Design for Transverse Forces	Considers web buckling, web crushing, and web crippling	Considers web buckling and web crushing, but not web crippling
Web Buckling	Guidance on the length of buckling is not given for fully restrained beams.	Slenderness is suggested to be $2.5d/t$ for fully restrained beams
Web Crushing	More conservative due to theoretically derived design formulae	Less conservative due to empirically derived design formulae

Table 1: Comparison of design methods for EC3 and BS5950 – 1 [16,17].

The depth of the section and the opening diameter, d, were fixed, having values of 449.8mm and 315mm ,,respectively. The beam depth to opening ratio, $D/d = 1.43$, was also fixed. The web thickness was taken to be 7.6mm and S/d was set at 1.6, for widely spaced web openings. The element type used in the existing analysis was SHELL181 with 4-noded plastic shell elements, and 6 degrees of freedom at each node. The material used was S355 grade steel with a Young's Modulus of 200GPa and Poisson Ratio, v, of 0.3. The material was assumed to behave elastically with a Young's Modulus of $E_1 = 200$GPa until the material reached a stress value of 355MPa. At the post-yielding zone, the tangent modulus was $E_2 = 2.00$GPa. Additionally the material was modelled using the Von Mises stress criterion, with a kinematic hardening plasticity model. The mesh type chosen was a free quadrilateral meshing for the web, and a mapped quadrilateral meshing for the flanges. An example of the type of mesh developed is shown in **Figure 1**. The mesh was examined for its appropriateness. It can be seen that the finer elements are developed near the edges, while course ones are shown towards the inside of the model where the stress is expected to be low. With this configuration the resulting stresses will be accurate and uniformly distributed across the beam model.

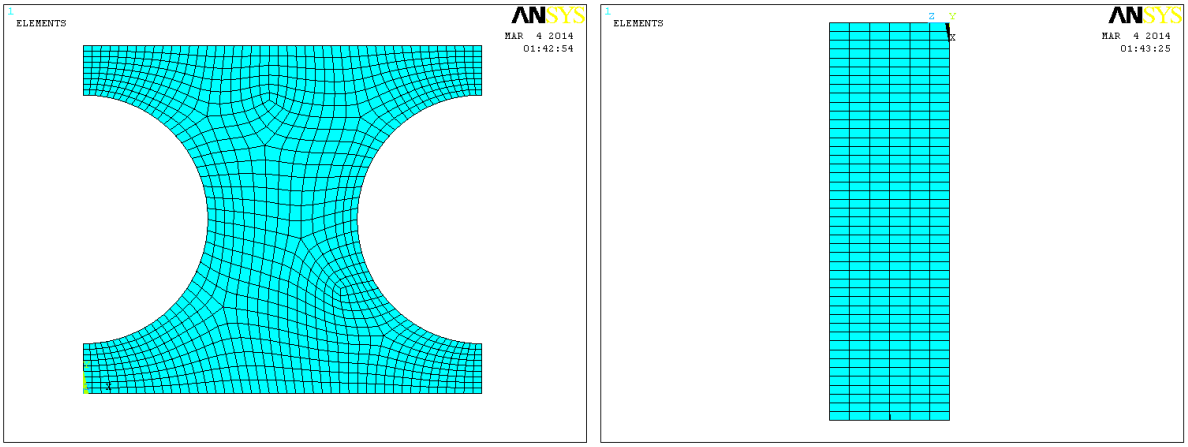

Figure 1: Free type mesh for the web (left) and mapped type mesh for the flanges (right).

It is important to define the boundary conditions of the short local model correctly, similarly to the literature [5]. Accordingly, the model is also assumed to have a pinned connection between the web and the flange. The boundary conditions are shown in **Table 2**:

Location	UX	UY	UZ	ROTX	ROTY	ROTZ
Flange(LHS)	Fixed	Free	Fixed	Fixed	Free	Fixed
Web(LHS)	Fixed	Fixed	Fixed	Fixed	Fixed	Free
Flange(RHS)	Free	Free	Fixed	Fixed	Fixed	Fixed
Web(RHS)	Free	Load	Fixed	Free	Fixed	Fixed

Table 2: Boundary conditions for models. LHS and RHS are left and right hand sides respectively. Source: [5].

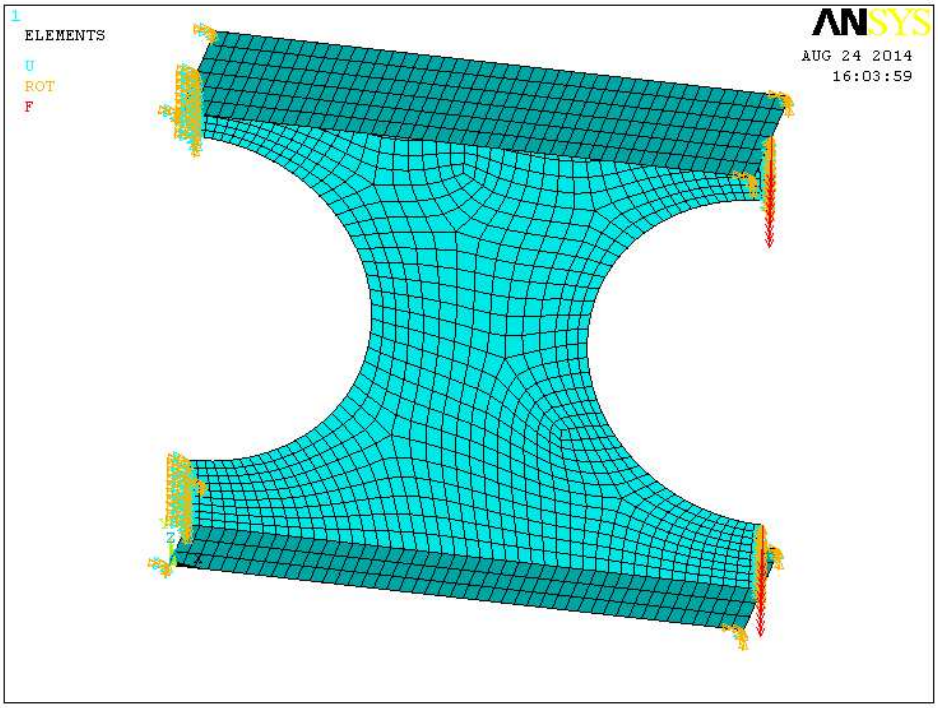

Figure 2: Model replication in ANSYS with ratio of $S/d = 1.6$, loads and constraints applied.

The procedure to obtain a nonlinear solution for the section above consisted of three stages. Firstly, a static solution with small displacements was obtained. Secondly, an Eigen buckling analysis was made, using that static solution. The third and final stage of obtaining the nonlinear solution initially consisted of updating the geometry of the model to the new deformed shape based on the first Eigen mode shape to take into account initial imperfections that would trigger the model to fail in a realistic manner. Then, what followed was the carrying out of a nonlinear (material and geometry) static analysis with large displacements for the updated section. The maximum load was recorded and compared to the model from the previous finite element analysis found in the literature and validated against an experimental physical test.

The initial imperfections were chosen to have a maximum amplitude of $t_w/200 = 7.6\text{mm}/200 = 0.038\text{mm}$. The Newton–Raphson method was enabled to avoid bifurcation points. In order to find a value for the failure load, different values of shearing force were applied. The maximum load resulted to be 248.25kN.

In **Figure 3**, a comparison of the Von Mises stresses between the model from the literature and the current working model was established and good agreement is shown.

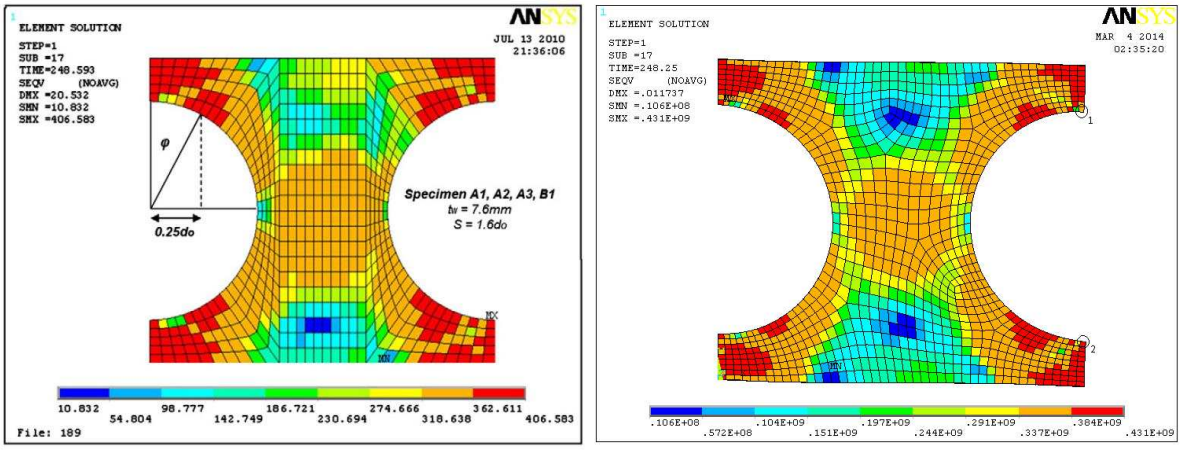

Figure 3: Original FEA experiment (left), and validation in ANSYS 11(right) [5].

The formation of plastic hinges due to Vierendeel moments at a $0.25d$ distance from the centre-line of the opening is also verified in the validated model. The value of the maximum load with fully converged models for both specimens is very close; 248.593kN for the original model and 248.25kN for the validated one.

In addition to the above, a mesh convergence study was made to show that the solution obtained was accurate. Different meshes with average element sizes of 50mm, 40mm, 30mm and 20mm were created and the Von Mises stresses were recorded at maximum loads at a point near the centre of the web-post. For the 50mm element size, the Von Mises stress was obtained as 361.2MPa, for 40mm as 356.7MPa, for 30mm as 358.1MPa and for 20mm as 355.4MPa. Therefore, the size choice can be treated as reliable.

3. Finite Element Method Analysis

A comprehensive parametric FE study was carried out to determine the buckling strength of cellular beams with double concentric transverse stiffeners on both sides of the web. The parameters altered were the S/d ratio, the web thickness, t_w, and the stiffener thickness, t_s. The results obtained were compared with existing results from previous studies of cellular beams without stiffeners [5].

3.1 Model Characteristics

The material properties used for the beam model and the stiffeners was chosen to be bilinear isotropic. Steel grade S355 was used ($f_y = 355$MPa, $f_u = 510$Mpa). The tangent modulus was assumed to be 580MPa, similar to the parametric study presented in the literature [5]. This realistic approximation was employed as a tangent modulus of 2000MPa similar to the validation study produced non-convergence issues in the computational models.

The UB 452 x 157 x 52 cross-section was used again. The stiffeners were designed with a typical chamfer size of 20mm at the top and bottom, between the flange and web connection. The boundary conditions were kept the same as for the validation model, modelling the connections between the flange and the web as pinned. Fully mapped mesh was developed to capture and control all the details of the models. Moreover, the maximum element size was chosen to be not greater than 15mm. This was done to increase the quality of the results and to enable accurate selection of specific points when comparing the results afterwards. The meshed sections are shown in **Figure 4**.

The ratio S/d was examined for values of 1.1, 1.2 and 1.3. The distances between the centres of the circular perforations were 346.5mm, 384mm and 409.5mm, respectively. Various web thicknesses were examined such as 5mm, 7.6mm and 10.5mm. Typical stiffener thicknesses of 5mm, 10mm and 15mm were examined. A total of 31 analyses were performed. Except from the planned 27 tests, an additional analysis for a model with $S/d = 1.4$, $t_w = 5$mm, $t_s = 15$mm was carried out, to demonstrate the lack of effectiveness of a transverse stiffener for higher S/d ratios. The remaining three analyses, regarded models without stiffeners with a web thickness of 7.6mm, and S/d ratios of 1.1, 1.2, 1.3, in order to demonstrate the delay of plastic deformation due to the addition of stiffeners.

Similarly to the validation study, initial imperfections were added to the models in order to obtain the out-of-plane buckling displacements. The initial imperfections had a maximum amplitude of $t_w/20$; thus $5mm/200 = 0.025$mm, $7.6mm/200 = 0.038$mm and $10.5mm/200 = 0.0525$mm for each web thickness, respectively.

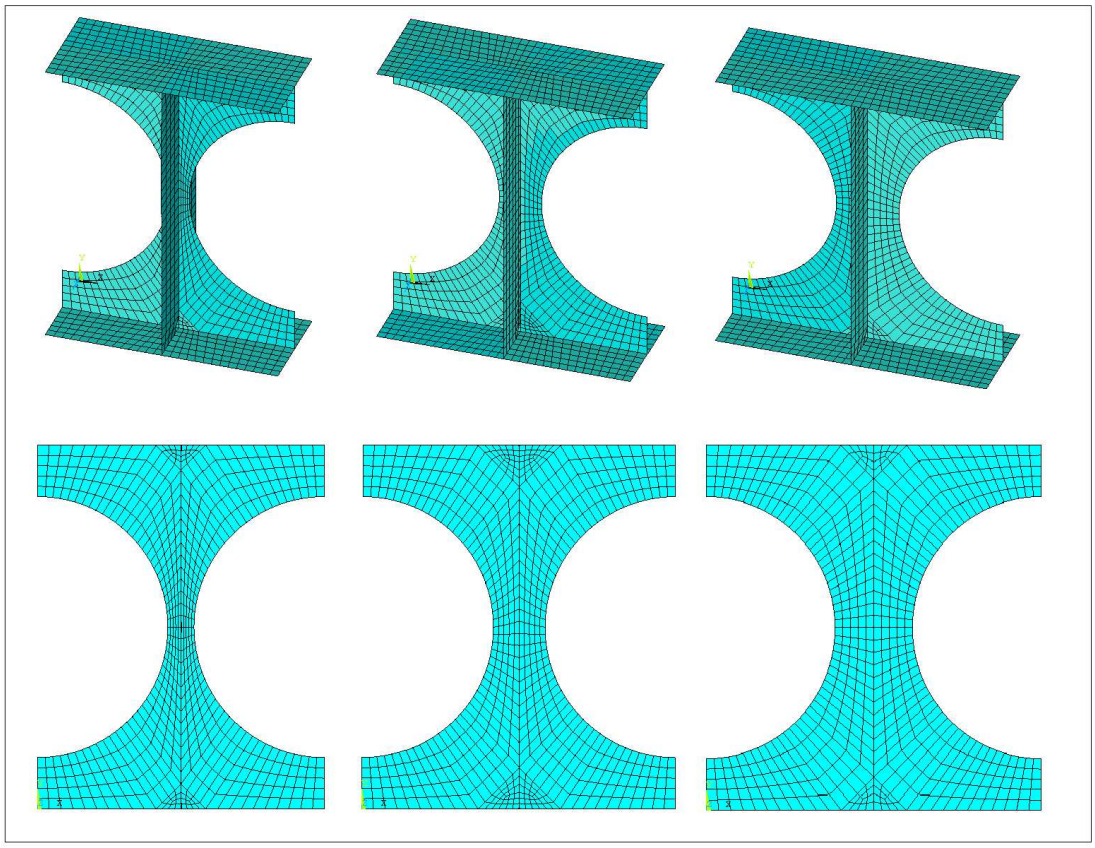

Figure 4: Mapped meshed models with $S/d = 1.1, 1.2$, and 1.3 ratios respectively.

3.2 Test results - Discussion

3.2.1 Strength against Parameters

The vertical and out–of–plane deflections were monitored throughout the FE analyses and two modes of failure were clearly observed. The first and most common type was the material failure, where the ultimate strength was reached. The second mode observed was the buckling failure, in which the beam very rapidly achieved large deformations in the out–of–plane direction of the web-post, the analyses also stopped before the ultimate strength was reached. **Figure 5** to **Figure 7** display the maximum non-convergent load carrying capacities for all, including the tests with no stiffeners, as published in the literature [5].

From these figures it was observed that the beams with stiffened openings demonstrate an increase in strength as was anticipated. It is also clearly demonstrated that the maximum strength is also dependent on other geometric properties as the effect of the stiffeners was not uniform across the tests with other variables. Considering the web thickness, it was observed that the stockier webs benefitted more from the stiffeners than the slender webs did. For instance, the maximum strength increase for a web thickness of 5mm was 53kN, whereas for a web thickness of 7.6mm, it was 70kN.

Considering the thickness of the stiffener, it appeared that in most cases there was a gain in strength when the thickness of the stiffener was increased. However, in some cases, the increase in thickness of the stiffener did not imply an increase in strength (eg. for the web thickness of 5mm and for $S/d = 1.1$). Potentially, the specimen had already reached the maximum strength with the use of stiffeners. For the case of $S/d = 1.3$, the slenderness of the web played an

important role, as well as the spacing of the web openings, as it can be seen from **Figure 5** to **Figure 7**.

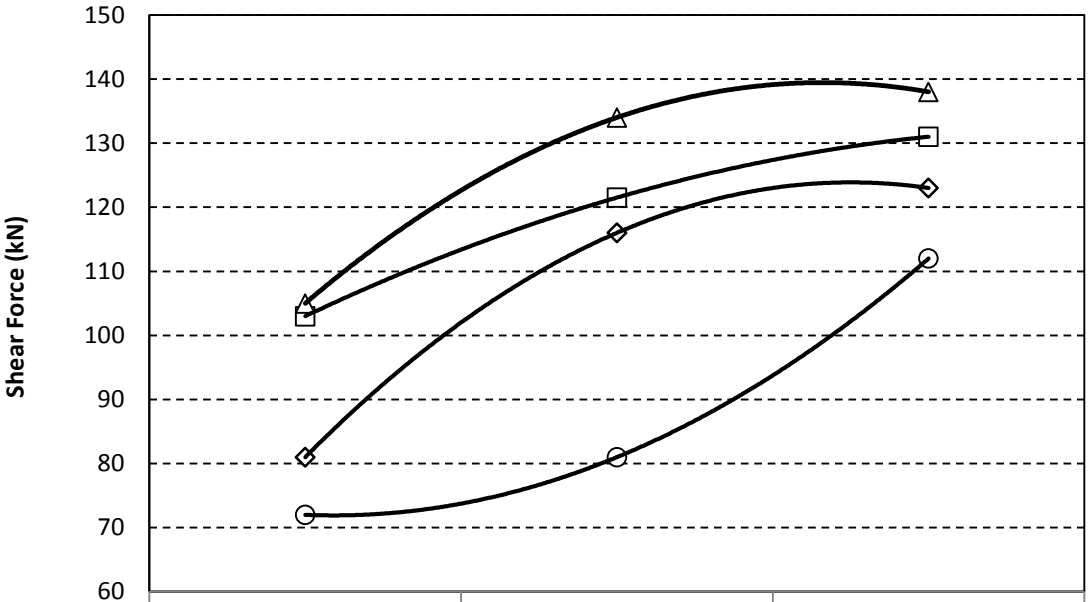

	1.1	1.2	1.3
○ No stiffener	72	81	112
◇ ts = 5mm	81	116	123
□ ts = 10mm	103	121.5	131
△ ts = 15mm	105	134	138

Figure 5: Vierendeel Shear Force against S/d ratio, for web thickness of 5mm and for stiffener thicknesses of 5mm, 10mm, 15mm.

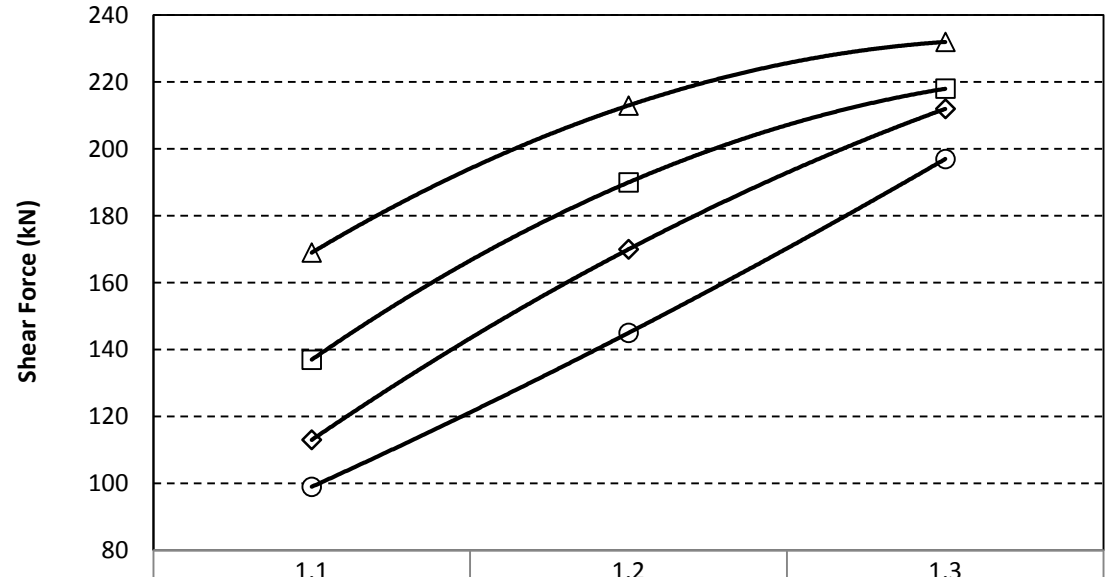

	1.1	1.2	1.3
○ No stiffener	99	145	197
◇ ts = 5mm	113	170	212
□ ts = 10mm	137	190	218
△ ts = 15mm	169	213	232

Figure 6: Vierendeel Shear Force against S/d ratio, for web thickness of 7.6mm and stiffener thicknesses of 5mm, 10mm and 15mm.

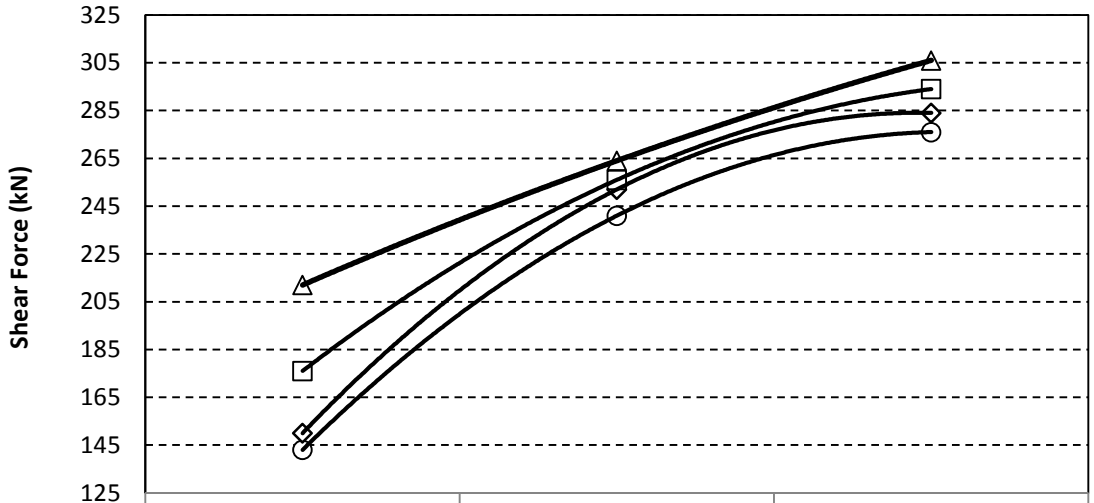

	1.1	1.2	1.3
○ No stiffener	143	241	276
◇ ts = 5mm	150	252	284
□ ts = 10mm	176	256	294
△ ts = 15mm	212	264	306

Figure 7: Vierendeel Shear Force against S/d ratio, for web thickness of 10.5mm and stiffener thicknesses of 5mm, 10mm and 15mm.

Regarding the web opening spacing, S/d, it was evidenced that there was a reduction in the increase of the maximum load carrying capacities as S/d was increased, and this was applied for all models studied. It is worth noting that in the case where $S/d = 1.3$, the contribution to strength from the stiffener was not significant and hence, in terms of design, it would be appropriate to find another way of stiffening the web opening against shear.

Contour plots display the Von Mises stresses for all possible S/d ratios with the same web and stiffener thicknesses, as it is shown in **Figure 8**. It is demonstrated, that when S/d was equal to either 1.1 or 1.2, high compression and tension stresses developed in the web-post and were then transferred to the stiffener. On the other hand, when S/d was taken equal to 1.3, the section would reach maximum load before the strength of the stiffener was fully utilised.

In order to determine a limit below which a transverse stiffener would be effective, further research was conducted. A model with $S/d = 1.4$ was designed and tested for $t_w = 5$mm, and $t_s = 15$mm. The model was initially compared at maximum capacity load with the results found in the literature [5]. The unstiffened version of this model, with $t_w = 5$mm, resisted about 130kN. When the same model was tested with a stiffener of 15mm thickness, the maximum capacity was only increased to 141kN. This is clearly a lower contribution compared to those achieved for the same web thicknesses and smaller S/d ratios.

At $S/d = 1.4$ it was further noticed, that the web buckled prior to the development of high stresses in the stiffener. It is anticipated that for even higher values of S/d, the contribution of the transverse stiffener will be further reduced. The recommended upper limit of S/d when strengthening cellular beams with double concentric transverse intermediate stiffeners, is equal to 1.3.

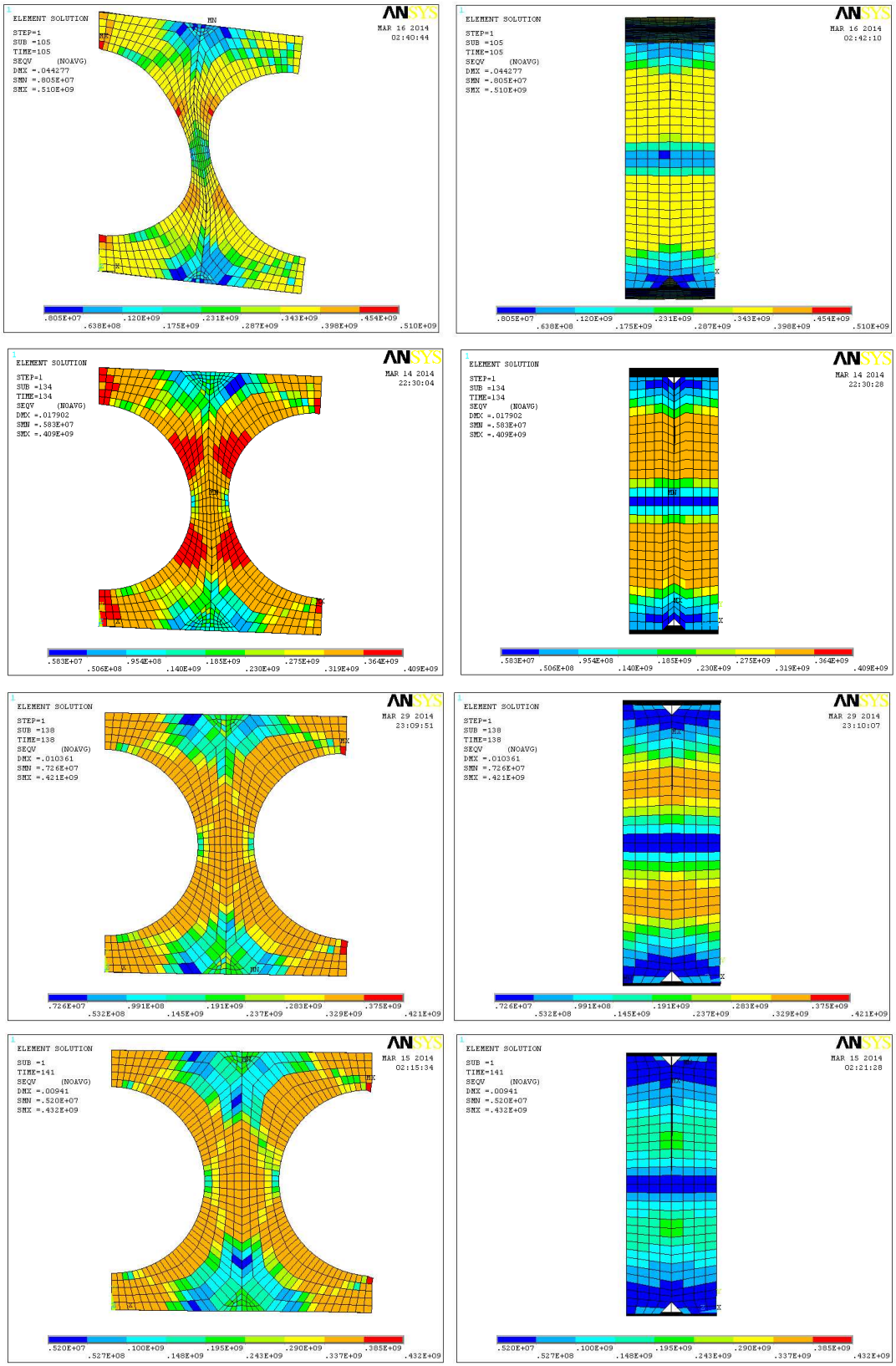

Figure 8: Web and Stiffener elevations, $S/d = 1.1, 1.2, 1.3, 1.4, t_w = 5mm, t_s = 15mm$.

The type of failure mode was also examined. The failure mode was either through buckling or Vierendeel shearing, dependent on the geometric parameters selected. The failure modes of the

FE analyses are presented in **Table 3**. It is observed that almost all buckling modes occurred at $S/d = 1.3$, with only one buckling failure mode taking place in the case of $S/d = 1.2$.

The stiffeners were provided to prevent buckling in the out-of-plane direction of the web. Since models with $S/d = 1.3$ failed primarily due to buckling, it can be inferred that transverse stiffeners are ineffective for such a beam. The stiffener contribution to the strength of the beams with $S/d = 1.3$ was significantly less than the contribution to beams with $S/d = 1.1$ and 1.2, as it was highlighted earlier.

t_w(mm),	t_s(mm)	$S/d = 1.1$	$S/d = 1.2$	$S/d = 1.3$
5	5	Vierendeel	Vierendeel	Vierendeel
	10	Vierendeel	Vierendeel	Vierendeel
	15	Vierendeel	Buckling	Buckling
7.6	5	Vierendeel	Vierendeel	Buckling
	10	Vierendeel	Vierendeel	Buckling
	15	Vierendeel	Vierendeel	Buckling
10.5	5	Vierendeel	Vierendeel	Buckling
	10	Vierendeel	Vierendeel	Buckling
	15	Vierendeel	Vierendeel	Vierendeel

Table 3: Section failure modes, depending on the parameter examined. 20 out of 27 models had a Vierendeel shearing failure mode, and only 7 had a buckling failure mode.

3.2.2 Incremental Shearing

Initially, it was observed that the stresses produced were primarily formed entirely in the web. Then, post-yielding stresses were located at the position of the plastic hinges in the vicinity of the web openings. Following that, stresses started to be distributed in the stiffeners, starting from the same level of the plastic hinges and then spreading in the vertical plane both upwards and downwards. It is worth mentioning that the use of the stiffeners caused an observable delay in the buckling or yielding for most of the specimens. During this delay, the high stresses in the web were increased gradually, while the stresses in the stiffeners increased rapidly. Upon reaching the maximum stress capacity of the stiffeners, plastic hinges formed, and the specimens failed either by reaching the maximum load carrying capacity or by excessive web buckling.

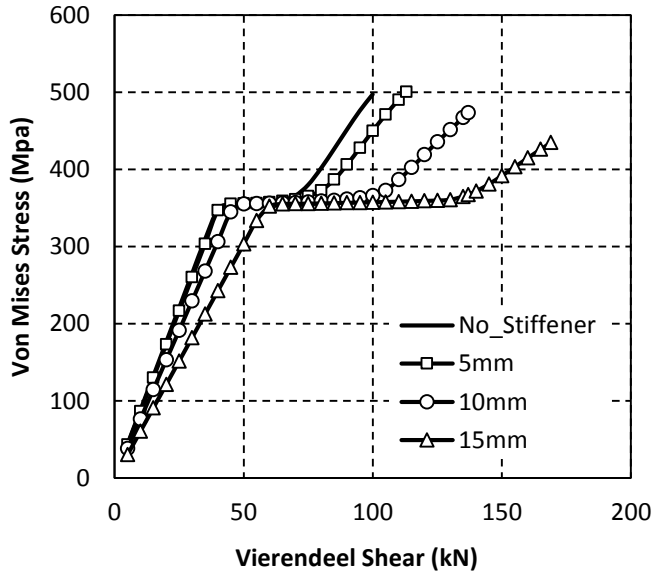

Figure 9: Stress against Shear graph for $S/d = 1.1, t_w = 7.6mm$ for different stiffener thicknesses.

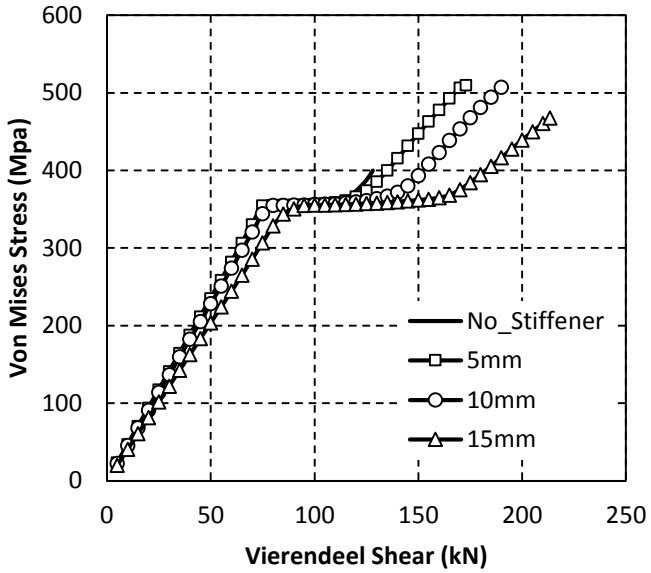

Figure 10: Stress against Shear graph for $S/d = 1.2, t_w = 7.6mm$ for different stiffener thicknesses.

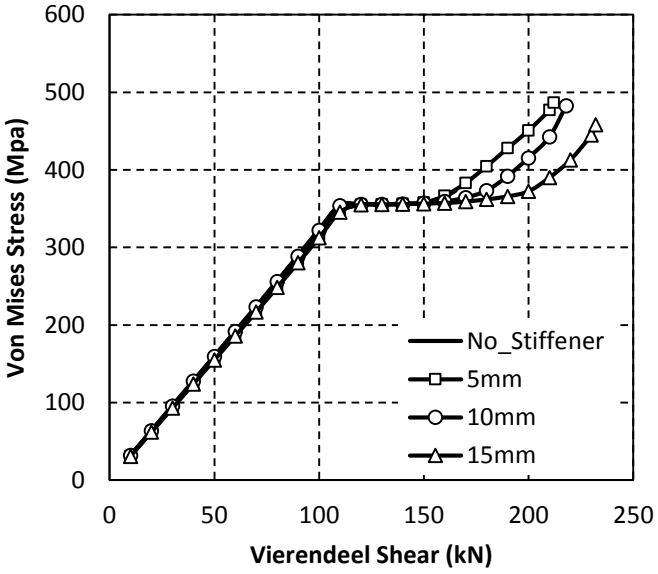

Figure 11: Stress against Shear graph for $S/d = 1.3$, $t_w = 7.6mm$ for different stiffener thicknesses.

From **Figures 9**, **10** and **11** it was observed that the aforementioned delay in yielding was more noticeable for higher stiffener thicknesses and for lower S/d ratios. In **Table 4**, the load levels in which these stages were observed are summarised. In **Figures 12** and **13**, snapshots for two of the specimens for all mentioned stages are shown. **Figure 12** shows a case where the mode of failure is Vierendeel shearing, while **Figure 13** demonstrates a failure mode of buckling.

$t_w(mm), t_s(mm)$	$S/d = 1.1$			$S/d = 1.2$			$S/d = 1.3$		
	YL	**SFUS**	**Max**	**YL**	**SFUS**	**Max**	**YL**	**SFUS**	**Max**
5, 5	30	58	81	57	91	116	97	107	123
5, 10	34	72	103	45	107.5	121.5	78	98	131
5, 15	31	74	105	59	129	134	76	100	137
7.6, 5	41	82	113	85	112	170	112	168	212
7.6, 10	47	95	137	63.3	135	190	114	174	218
7.6, 15	55	113	169	63.3	151.7	213.3	82	186	232
10.5, 5	56	104	150	102	148	252	194	224	284
10.5, 10	60	116	176	82	172	256	160	226	294
10.5, 15	70	138	212	84	188	264	116	238	306

Table 4: Loading behaviour for sections. YL = Yielding Load (kN), SFUS = Stiffener Full Utilization Strength (kN), Max = Maximum Load Measured (kN).

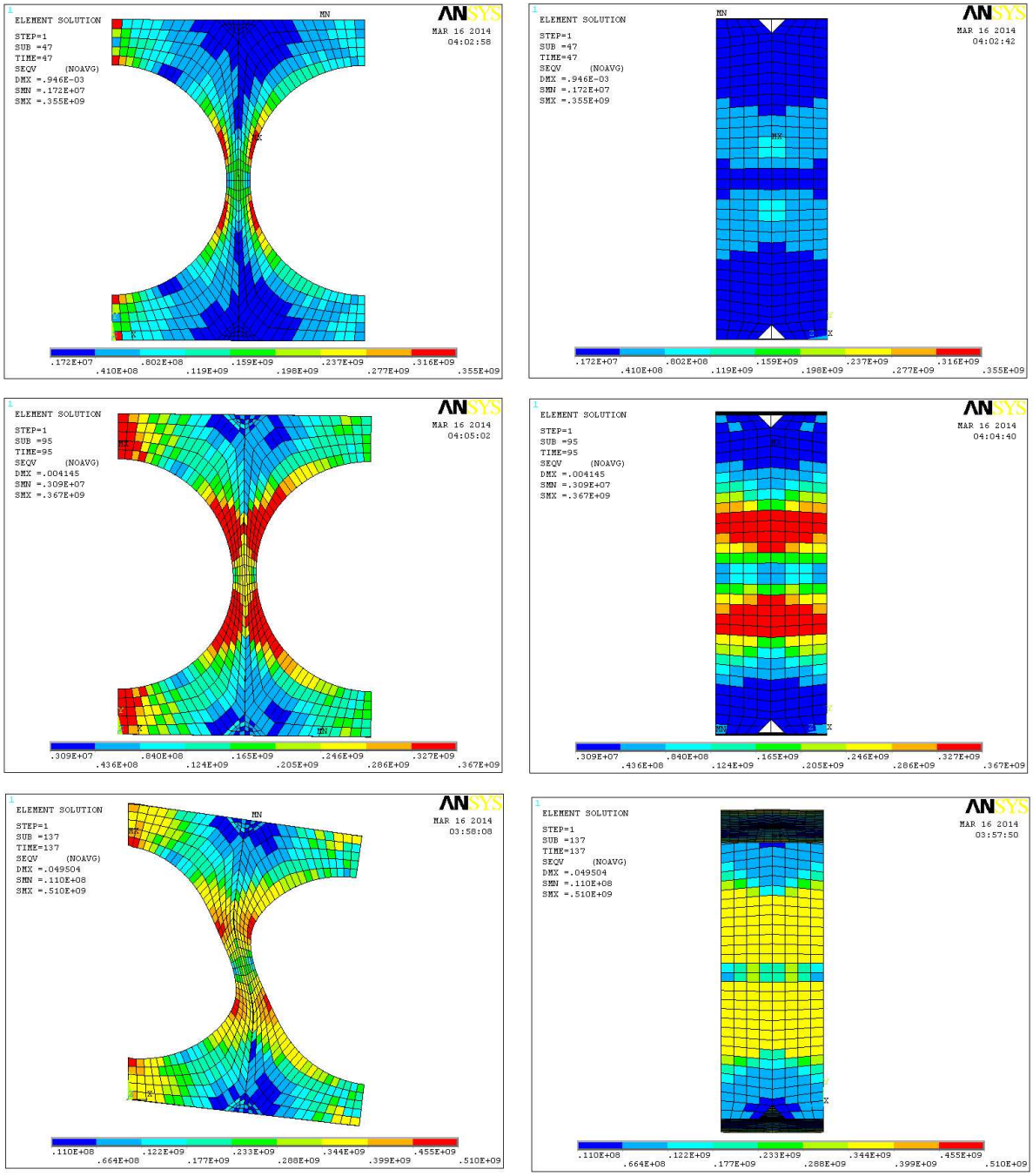

Figure 12: Snapshots of model with parameters $S/d = 1.1, t_w = 7.6\text{mm}, \ t_s = 10\text{mm}$. The failure mode is Vierendeel shearing. Top: at yielding load. Middle: at full utilization of stiffener. Bottom: at maximum measured load.

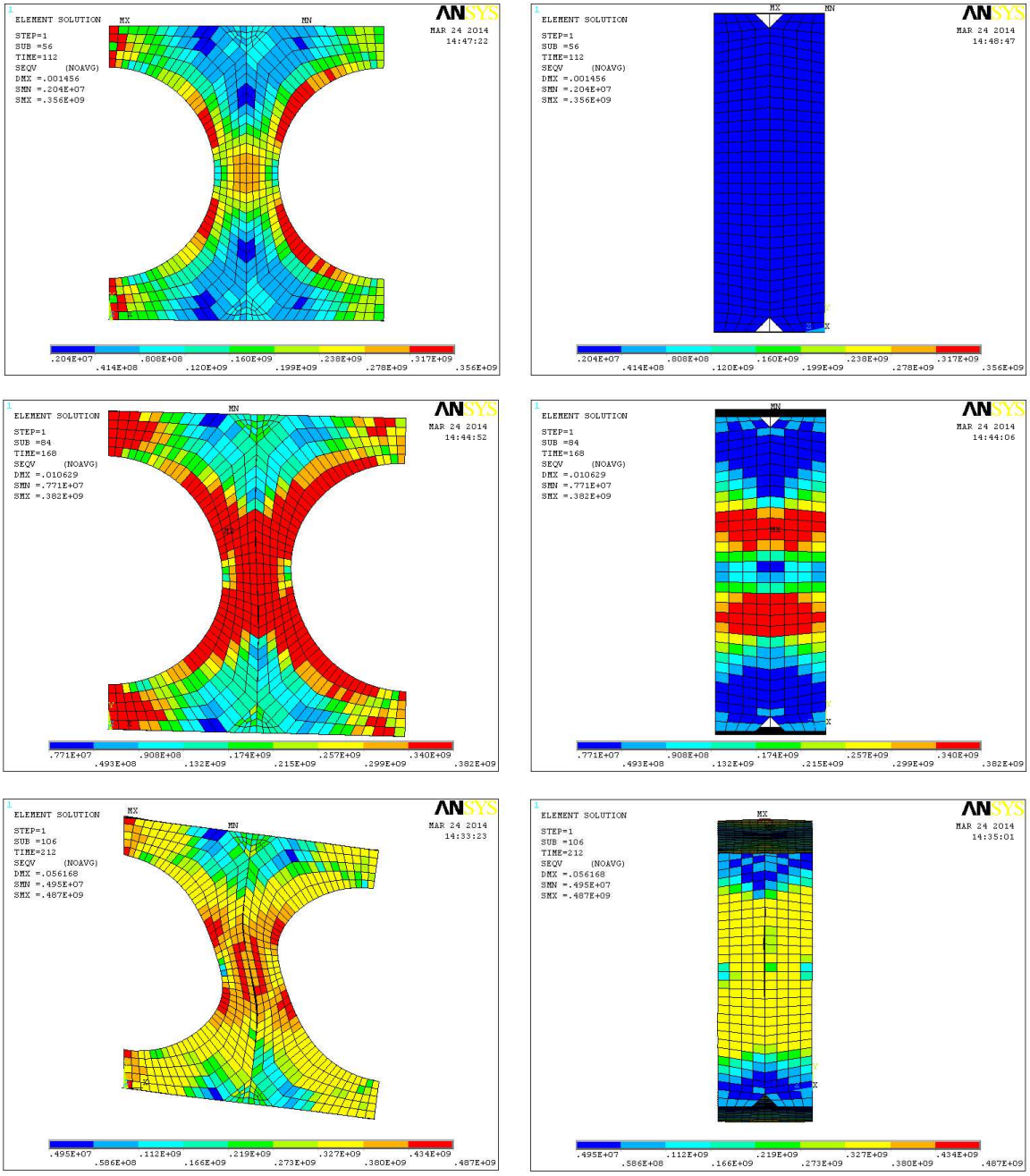

Figure 13: Snapshots of model with parameters $S/d = 1.3, t_w = 7.6\text{mm}, t_s = 5\text{mm}$. The failure mode is buckling. Top: at yielding load. Middle: at full utilization of stiffener. Bottom: at maximum measured load.

3.2.3 Out–of–plane and Vertical Deflections against Loading

The vertical and out–of–plane deflections were measured at the points where plastic hinges in the openings were formed. These points are depicted in **Figure 14**.

During the Eigen buckling analysis, three different buckling deformation patterns resulted and they are affected the magnitude of the out–of–plane deformations observed by the specimens.

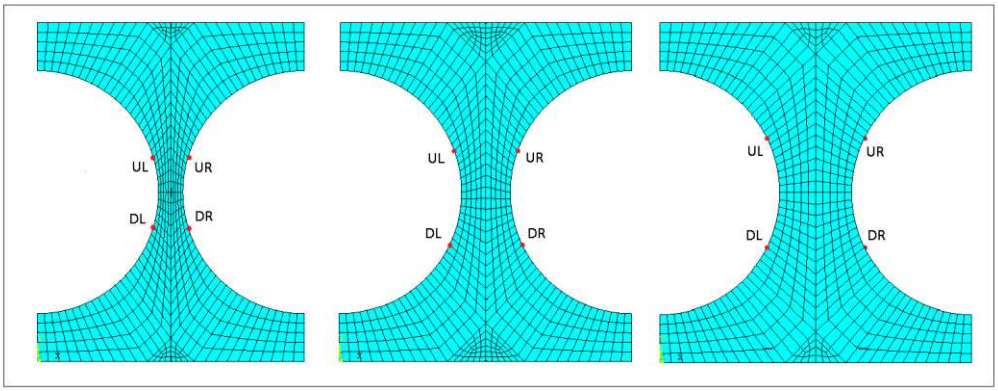

Figure 14: Points of measuring vertical and out – of – plane deflections. UL = Up Left, UR = Up Right, DL = Down Left, DR = Down Right.

The first buckling pattern can be seen in **Figure 15**. Such a pattern only takes place when the thickness of the stiffener is higher than the thickness of the web. When a very rigid stiffener was used, the deformation was concentrated on the upper right side of the specimen as it is shown in the figure and labelled herein as pattern A.

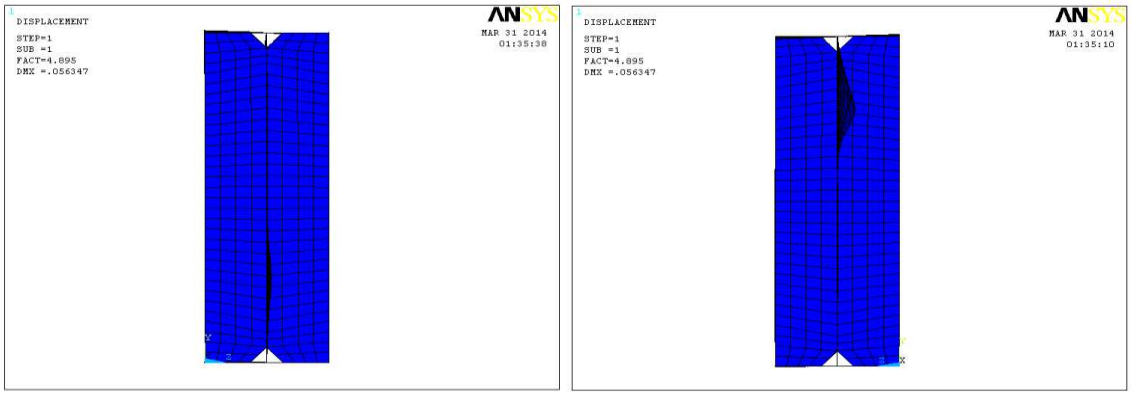

Figure 15: Buckling pattern A. UR and DR measure points can be seen from the image on the right, UL and DL measure points can be seen from the image on the left. The model shown is $S/d = 1.3, t_w = 10.5\text{mm}, t_s = 15\text{mm}$.

The second buckling pattern observed occurs when the thickness of the stiffeners is equal or less than the thickness of the web. This type of buckling usually involves concentration of the deformation towards the measure point DR when $S/d = 1.3$. This pattern is labelled as B, and it is shown in **Figure 16**.

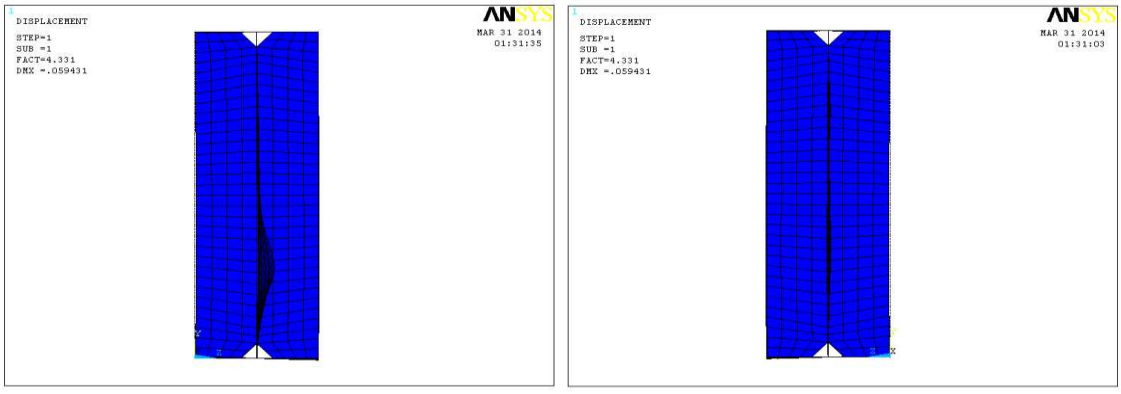

Figure 16: Buckling pattern B. UR and DR measure points can be seen from the image on

the right, UL and DL measure points can be seen from the image on the left. $S/d = 1.3$, $t_w = 10.5\text{mm}, t_s = 10\text{mm}$.

The third buckling pattern, labelled pattern C, occurred only for $S/d = 1.1$ and 1.2 and did not involve any noticeable out–of–plane movement of the stiffeners. Pattern C can be seen in **Figure 17**.

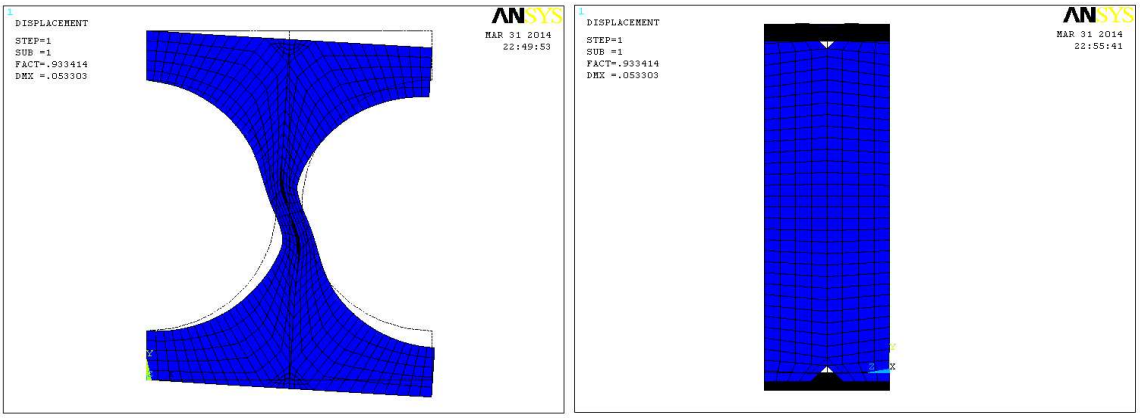

Figure 17: Buckling pattern C. UR and DR measure points can be seen from the image on the right, image of the distorted web is shown on the left. $S/d = 1.1, t_w = 5\text{mm}, t_s = 5\text{mm}$.

The authors have tried to realise any correlation between the buckling patterns and the failure mode. Assessing **Tables 3** and **5**, it can be seen that 8 out of 20 specimens that had Vierendeel shearing as a failure mode lie within pattern A, 1 specimen within pattern B, and 11 specimens within pattern C. On the other hand, 4 out of 7 specimens that had buckling as a failure mode lie within pattern A, while the other 3 lie within pattern B. It was concluded that there is a relation between the Vierendeel shearing failure mode and pattern C buckling, as well as buckling failure mode and pattern B buckling. Pattern A buckling occurred both in Vierendeel shearing and buckling failure modes.

t_w(mm),	t_s(mm)	$S/d = 1.1$	$S/d = 1.2$	$S/d = 1.3$
5	5	**C**	**C**	**B**
	10	**C**	**A**	**A**
	15	**A**	**A**	**A**
7.6	5	**C**	**C**	**B**
	10	**A**	**C**	**A**
	15	**A**	**C**	**A**
10.5	5	**C**	**C**	**B**
	10	**C**	**C**	**B**
	15	**A**	**A**	**A**

Table 5: A, B and C patterns of out–of–plane deformation. It can be seen that when $t_w \geq t_s$, most of the cases followed pattern B, and when $t_w < t_s$ the most dominant pattern was A. Pattern C appears to depend on the S/d ratio.

For each test made, the maximum deflection of all four dials was measured. The results of this procedure are shown on **Table 6**.

It could be observed from Table 6 that the maximum out-of-plane deflections for $S/d = 1.1$ are generally of a lower magnitude than the maximum deflections for $S/d = 1.2$, and those of $S/d = 1.2$ of a lower magnitude than those for $S/d = 1.3$. This was anticipated, as buckling deformations are more likely to take place for larger S/d ratios. The reduced effectiveness of the

stiffeners when the S/d ratio is increased could also be a contributing factor for the increasing out–of–plane deformations.

t_w(mm),	t_s(mm)	$S/d = 1.1$	$S/d = 1.2$	$S/d = 1.3$
5	5	0.0000958	0.105	0.263
	10	0.0000381	**2.25**	0.119
	15	0.00710	0.255	0.093
7.6	5	0.000158	0.00142	1.75
	10	0.00746	0.000489	**3.73**
	15	**0.0166**	0.000342	2.87
10.5	5	0.0000840	0.00104	0.0607
	10	0.0000508	0.000410	0.0212
	15	0.00917	0.0396	0.111
Maximum		**0.0166**	**2.25**	**3.73**

Table 6: Maximum out–of–plane deflections (mm).

Comparing the out-plane-deflections results of the models with parameters $S/d = 1.3, t_w = 7.6\text{mm}, t_s = 5, 10, 15\text{mm}$ to the out–of–plane deflections of the specimen B1 found in the literature review [5], it can be concluded that the deflections of the tests presented in the current study are higher (3.73mm compared to about 0.5 – 1mm). However, it is worth noting that the displacements of the previous study were measured at the centre of the web-post, and not at the position of the plastic hinges. Nevertheless, the deformations were of the same magnitude.

When comparing **Tables 5** and **6** it is highlighted that pattern C demonstrate*s* the smallest out–of–plane deformations; somewhat larger deformations were observed for pattern B, and finally considerably higher deformations were observed for pattern A. Additionally, the mode of failure for $S/d = 1.3$ was primarily due to buckling. It becomes apparent that the effectiveness of the transverse stiffeners reduces when S/d increases.

Representative graphs of out–of–plane deformations against incremental loading for each pattern type A, B, and C are presented on **Figure 18** to **20**.

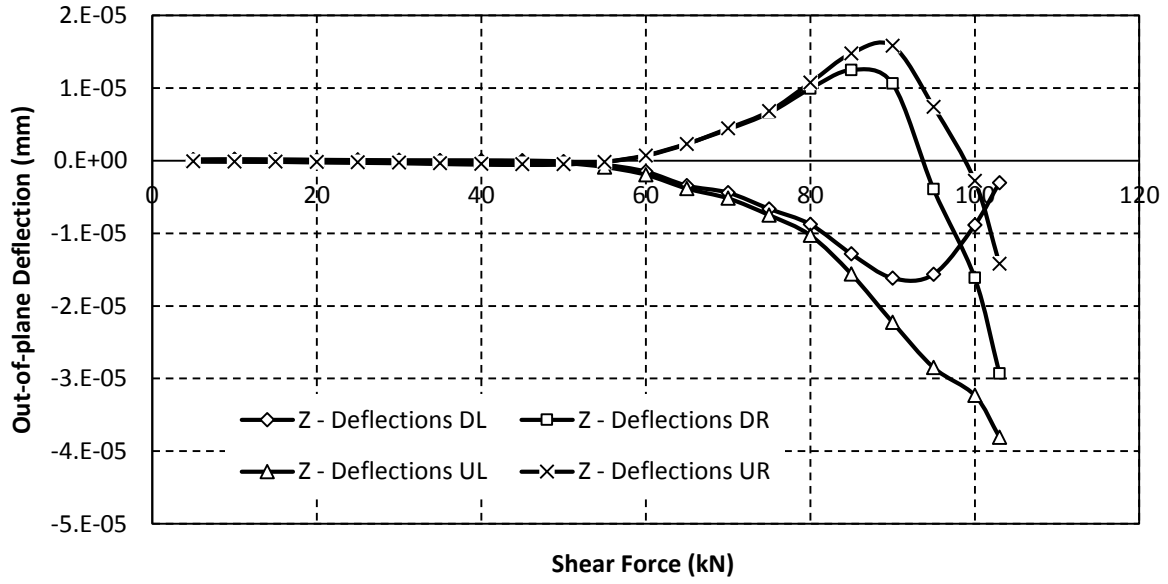

Figure 18: Representative out–of–plane deflections for pattern C. Deformations are negligible (S/d=1.1, tw=5mm, ts=10mm).

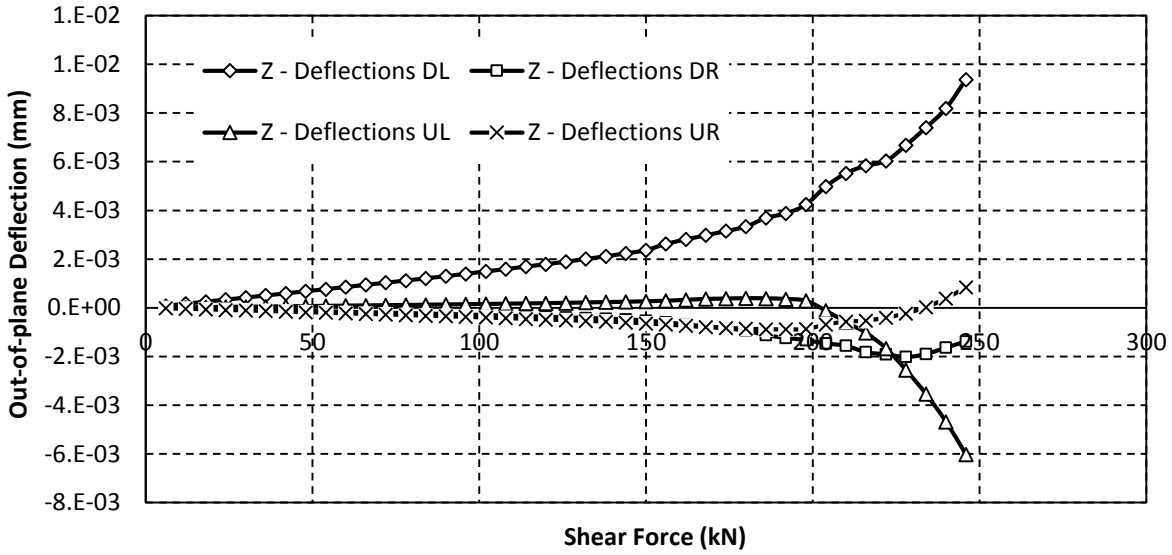

Figure 19: Representative out–of–plane deflections for pattern B. Deformations seem to be concentrated more on the lower left hinge, but they are still small (S/d=1.3, tw=10.5mm, ts=5mm).

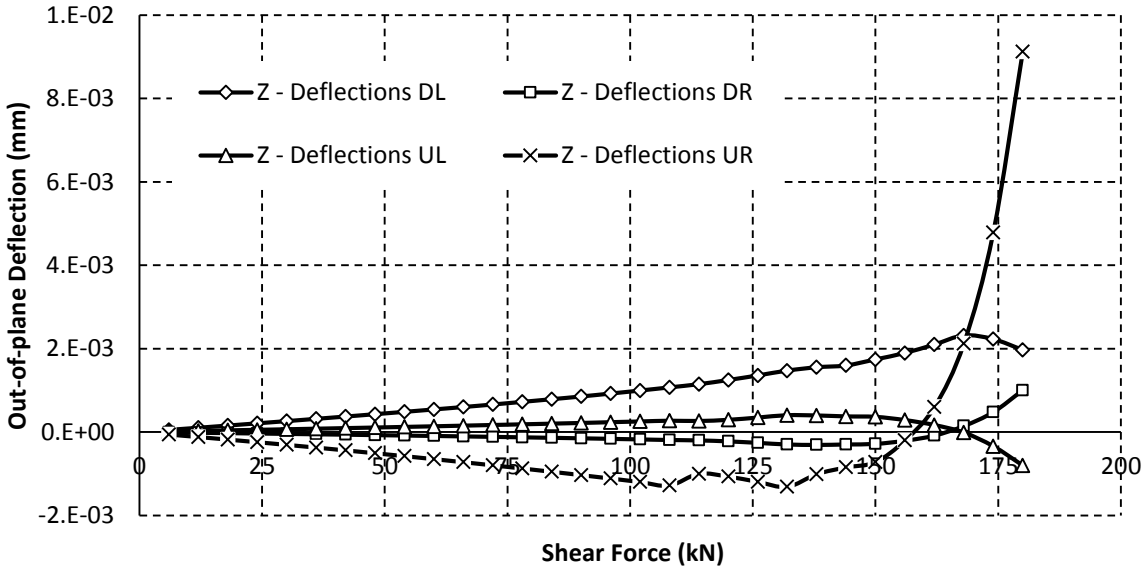

Figure 20: Representative out–of–plane deflections for pattern A. Deformations are concentrated on the upper right hinge, and are considerably higher than the previous cases (S/d=1.3, t_w=7.6mm, t_s=10mm).

When considering the above it is observed that an efficient way to increase the effectiveness of a transverse stiffener for larger S/d ratios may be to place the stiffeners with some eccentricity. If the stiffener thickness is higher than the thickness of the web, then the stiffener should be placed closer to the high moment side of the web. Conversely, if the stiffener thickness is lower than the thickness of the web, then the stiffener should be placed closer to the low moment side of the web. An illustration of this idea is depicted in **Figure 21**.

Following this design concept for larger S/d ratios, if a stiffener is thicker than the web it is more effective when it is placed like Type A. If the opposite is true, a Type B configuration would be a more effective design. It is worth stressing that this suggestion has not been proven further, but highlights prospective areas for future research and testing this statement's validity.

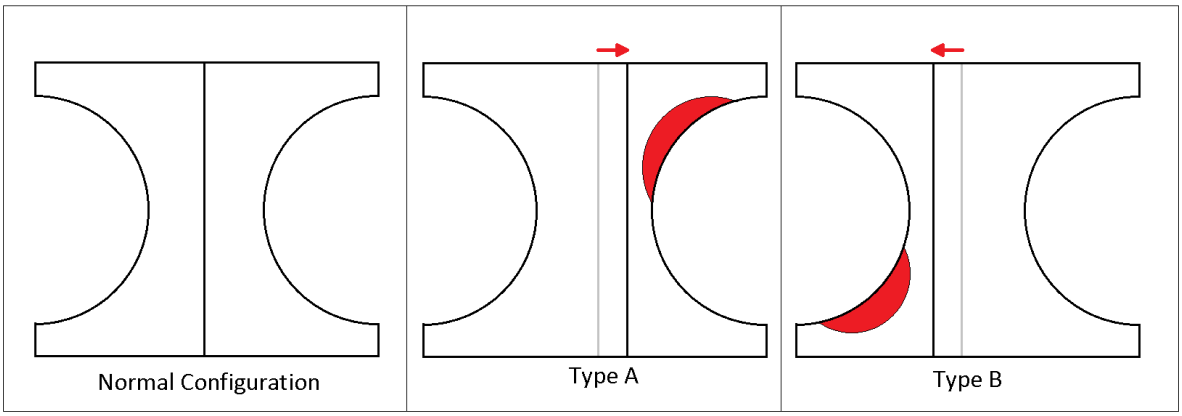

Figure 21: Left: Transverse stiffener with no eccentricity. Middle: Eccentricity for pattern A buckling. Right: Eccentricity for pattern B buckling. Highlighted areas: Areas where excessive buckling occurs.

Regarding the vertical deflections for each loading case, the maximum displacement for all four dials was chosen. For each S/d ratio, the maximum vertical deflections are shown in **Table 7** below:

t_w(mm)	t_s(mm)	$S/d = 1.1$	$S/d = 1.2$	$S/d = 1.3$
5	5	21.0	23.5	8.86
	10	21.7	16.1	5.91
	15	22.4	8.41	3.80
7.6	5	24.0	28.9	29.1
	10	24.4	**30.7**	27.2
	15	25.2	32.3	24.3
10.5	5	26.5	29.8	**30.0**
	10	26.7	30.3	28.9
	15	**28.1**	28.9	26.9
Maximum		**28.1**	**28.1**	**30.7**

Table 7: Maximum vertical deflections for the models tested. The units are in millimetres.

It is observed that there is no significant difference between the maximum vertical deflections for any S/d ratio studied. However, there was an increase in the maximum vertical deflection as the stiffener thickness increased for all the cases with $S/d = 1.1$. For $S/d = 1.2$ and 1.3 the opposite behaviour was noticed; when the thickness of the stiffener increased, the maximum vertical deflection was decreased. An exception was noticed for $S/d = 1.2, t_w = 10.5\text{mm}, t_s = 10\text{mm}$ where there was an increase of the maximum deflection. This meant that although the transverse stiffeners are designed to prevent buckling, they could reduce the vertical deflections too for certain cases.

It was also noticed that as the web thickness increased, the maximum vertical deflection increased as well. That was expected to happen, as a stocky web can withstand larger deformations before failure.

The results of $S/d = 1.3, t_w = 7.6\text{mm}, t_s = 5, 10, 15\text{mm}$ were compared with the results obtained from the laboratory experiment (specimen B1) of the previous work [5], which used the same S/d ratio and web thickness. As with the comparison of the out-of-plane deflections, the results corroborate; approximately 20–30mm deflection for both tests. The points measured for each test were at different positions, but not significantly enough to skew the data. **Figure 22** to **23** demonstrate the vertical deformations.

3.2.4 Plastic Hinge Formation and Effective Widths

It was interesting to examine how the transverse stiffeners would affect the formation of the plastic hinges for the specimens taken by the literature [5]. The plastic hinges, unlike the previous work, formed closer to the mid-depth of the web-post due to the use of stiffeners. Thus, while the effective width was $0.25d$ for an unstiffened section, for a stiffened section it becomes closer to $0.45d$.

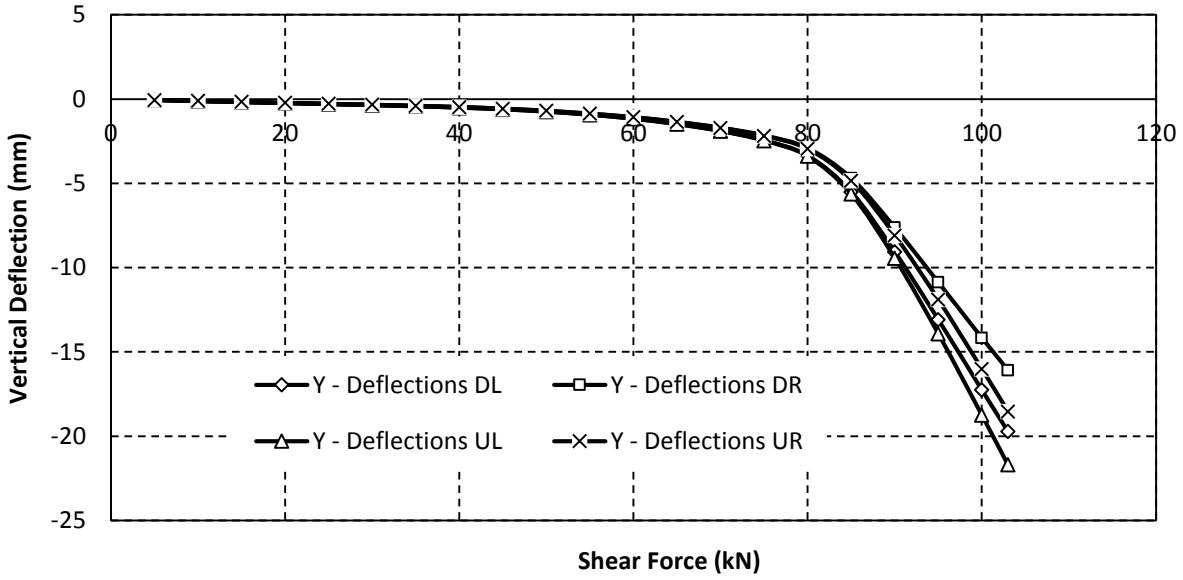

Figure 22: Representative graphs vertical deflection against Vierendeel shear (S/d=1.1, t_w=5mm, t_s=10mm).

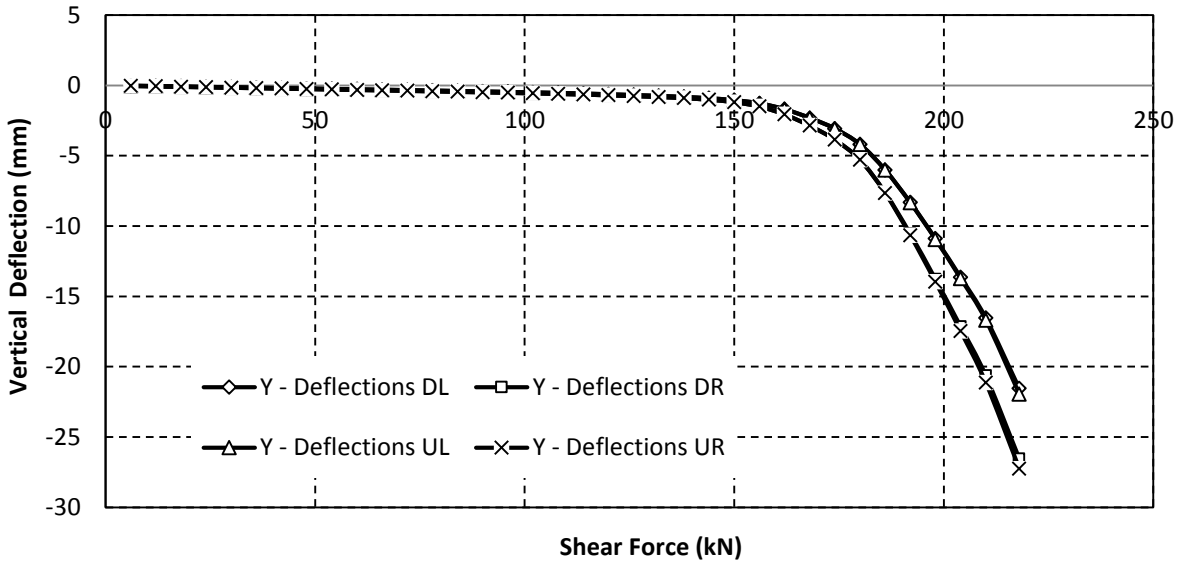

Figure 23: Representative graphs vertical deflection against Vierendeel shear (S/d=1.3, t_w=7.6mm, t_s=10mm).

The formation of the plastic hinges were not clearly visible in the Von Mises stress contour plots, such as in the case when $S/d = 1.3$ and $t_w = 5$mm. For this case, it was assumed that the plastic hinges formed in the same position as with all other specimens with $S/d = 1.3$. The calculated angles, φ^o, and the effective widths for each ratio S/d are synopsized in **Table 8**.

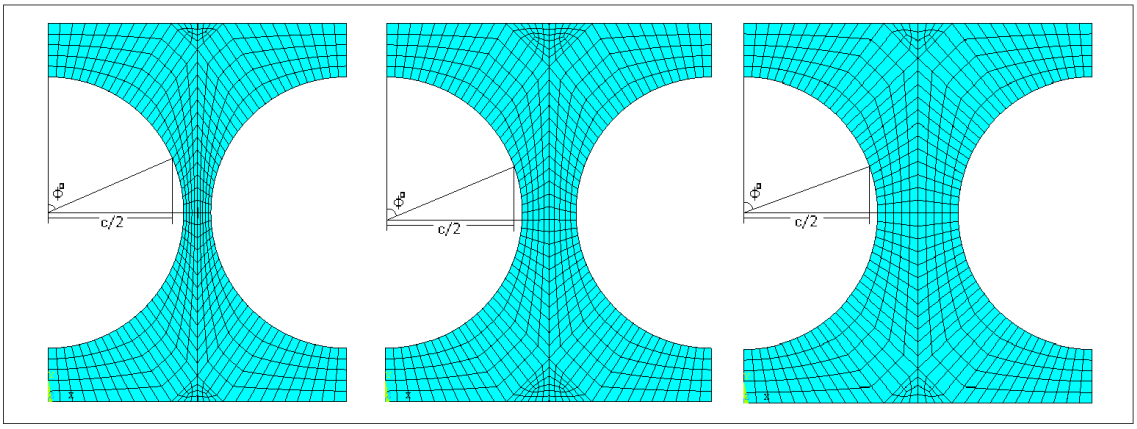

$S/d = 1.1$		$S/d = 1.2$		$S/d = 1.3$	
φ^o	$c/2$(mm)	φ^o	$c/2$(mm)	φ^o	$c/2$(mm)
71.37	$0.474d$ =149.26	68.67	$0.464d$ =146.31	67.5	$0.451d$ =141.92

Table 8: Angle φ^o and effective widths $c/2$ for all model S/d ratios. The effective widths are close to $0.5d = 175mm$, the length of the radius of the openings.

4. Design Model

The design model for this work was based on previous studies [2,5]. Since the design models of those studies considered unstiffened webs, various modifications took place in order to obtain reasonable results.

In previous works, a strut analogy with buckling curves of type C based on BS 5950–1:2000 [18] was used. In this analogy, it was considered that half of the Vierendeel shear force was

concentrated in the upper tee of the beam, and compressive stresses were produced by shear actions acting diagonally on the web-post, from the upper right tee to the lower left tee. The strut acting like a "column" with both ends fixed. Eurocode 3 also has a similar strut analogy, that could have led to a very similar design model as the one designed for this work. However, in this work, the strut analogy of BS 5950–1:2000 was selected to provide consistency with previous works [2,5].

In the present study, the stiffeners are considered to reduce the effective length of the strut by half for the cases where $S/d = 1.1, 1.2$. It is therefore as if the diagonal strut started from the upper right tee and ended on the stiffener. This implied that the length of the diagonal strut would not be $\sqrt{s_0^2 + d^2}$ but $\sqrt{s_0^2 + (0.5d)^2}$. The compressive stresses created by the Vierendeel mechanism are considered to be forming from the upper right tee, to the middle of the stiffener. The effective width of the strut, b_e, is taken as half the web-post width. The formula is now updated to:

$$\sigma = \frac{V_v}{2b_e t_w} = \frac{V_v}{2\frac{s_0}{2}t_w} = \frac{V_v}{s_0 t_w}$$

Where σ was the compressive stress in MPa, V_v was the Vierendeel shear force, s_0 the web-post width, and t_w the thickness of the web. To calculate the Vierendeel shear force, it is first necessary to calculate the effective length of the strut, using a reduction factor of 0.5, due to the assumed fixed–fixed conditions:

$$l_e = 0.5\sqrt{s_0^2 + (0.5d)^2}$$

The effective length is altered in the way demonstrated above for the cases when $S/d = 1.1, 1.2$. For the $S/d = 1.3$ case, the stiffeners are not fully utilised when failure occurred. To simulate this behaviour it is assumed that the stiffeners are acting as a pinned end for the strut.

Therefore, for:

$$S/d = 1.3$$
$$l_e = 0.7\sqrt{s_0^2 + (0.5d)^2}$$

Following that, the slenderness of the web-post can be calculated, using the formula:

$$\lambda = \frac{l_e\sqrt{12}}{t_w}$$

The slenderness values are used to find the buckling curves of type C which are necessary to give the compressive strength, p_c, of the web-post [18]. Then, the Vierendeel shear force is calculated by:

$$V_v = 2b_e p_c t_w = s_0 p_c t_w$$

Hence, the compressive strength is estimated as:

$$\sigma = \frac{V_v}{s_0 t_w} = p_c$$

The compressive stresses evaluated here are presented in **Table 9**:

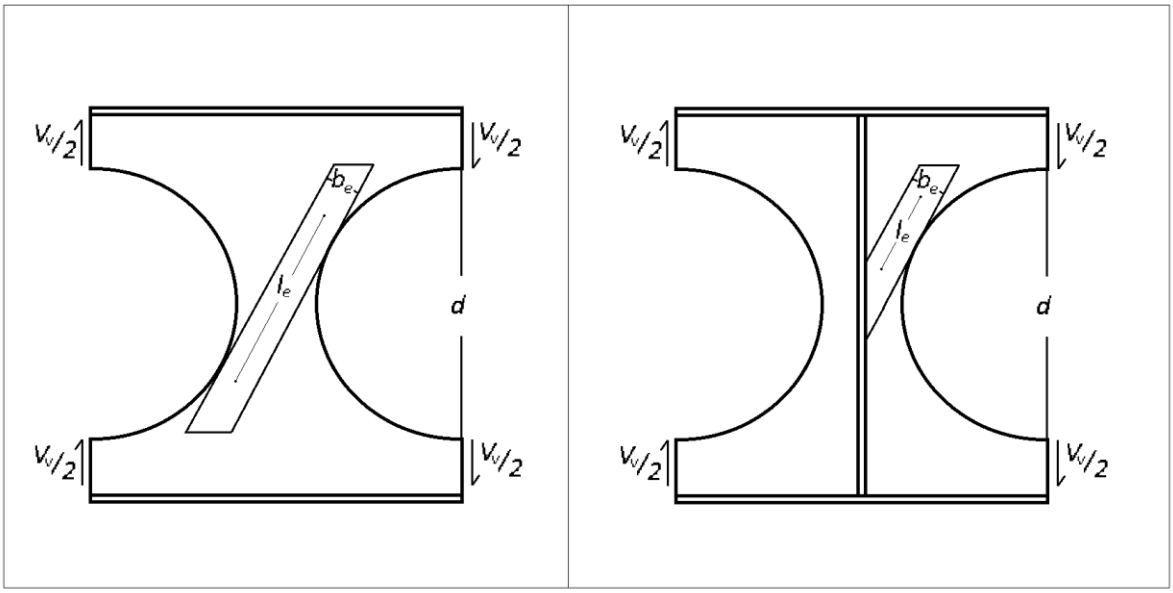

Figure 24: Strut analogy for unstiffened section (left) and for stiffened section (right). The stiffeners act as a fixed support for the strut for $S/d = 1.1, 1.2,$ and as a pinned support for $S/d = 1.3$.

S/d	1.1	1.1	1.1	1.2	1.2	1.2	1.3	1.3	1.3
t_w(mm)	5	7.6	10.5	5	7.6	10.5	5	7.6	10.5
σ(Mpa)	259	311	331	250	304.5	328	166	250	295

Table 9: Compressive stresses for the models studied, considering post buckling strength according to BS5950–1:2000[18].

t_w(mm)	t_s(mm)	$S/d = 1.1$	$S/d = 1.2$	$S/d = 1.3$
5	5	514.29	368.25	260.32
	10	653.97	385.71	277.25
	15	666.67	425.40	292.06
7.6	5	472.01	355.05	295.18
	10	572.26	396.83	303.54
	15	705.93	445.56	323.03
10.5	5	453.51	380.95	286.22
	10	532.12	387.00	296.30
	15	640.97	399.09	308.39

Table 10: Compressive stresses (MPa) from the results of the FEA.

The compressive stresses are calculated similarly to the procedure above, with the difference that the Vierendeel shear capacity is considered to be the failure load. These stresses are then compared with those found from the FE analysis results and **Table 10**. Comparing **Tables 9** and **10**, it is concluded that the compressive stresses from the FE analyses are considerably higher than those from BS5950–1 where $S/d = 1.1, 1.2$. For $S/d = 1.3$ the compressive stresses are close. Consequently, the values found from the FE analyses are considered to be very conservative and therefore not selected for the design model.

For the ratios $S/d = 1.1, 1.2$ the failure mode for the vast majority of the beams is the Vierendeel mechanism. Hence, the failure mode was governed by the Vierendeel bending capacity, and not

the web-post buckling capacity. For those S/d ratios, the approach used on previous studies has been adopted by practitioners and is recommended [2,5].

The Vierendeel shear capacity on the upper right tee was given by converting the circular openings to equivalent rectangular areas, with height, d, and critical opening, $a * d$, where $a = 0.45$. This approximated estimation for a due to the fact that the angle φ^o was very close in magnitude for all S/d ratios. The formula was as follows:

$$\frac{V_v}{2} = \frac{\mathrm{M}_{plastic}}{a * d}$$

For cases where the thickness is 5mm, the web was considered to be semi–compact, according to BS5950–1, and the elastic moment capacity was calculated instead in the equation above. The plastic moment capacity was calculated, as in the previous work [5]:

$$M_{plastic} = 0.5A_{tee}(0.5\bar{x}_1 + \bar{x}_2)p_y$$

Where:

$$A_{tee} = bt_f + d_T t_w$$

$$\bar{x}_1 = {A_{tee}}/{2b}$$

$$\bar{x}_2 = \frac{0.5(T - \bar{x}_1)^2 + d_T t_w((T - \bar{x}_1) + 0.5d_T)}{0.5A_{tee}}$$

$$d_T = (428 - 315) * 0.5 = 56.5\text{mm}$$

$$T = t_f - \bar{x}_1$$

Where b, t_f are the width and thickness of the flange, and d_T is the depth of the upper tee.

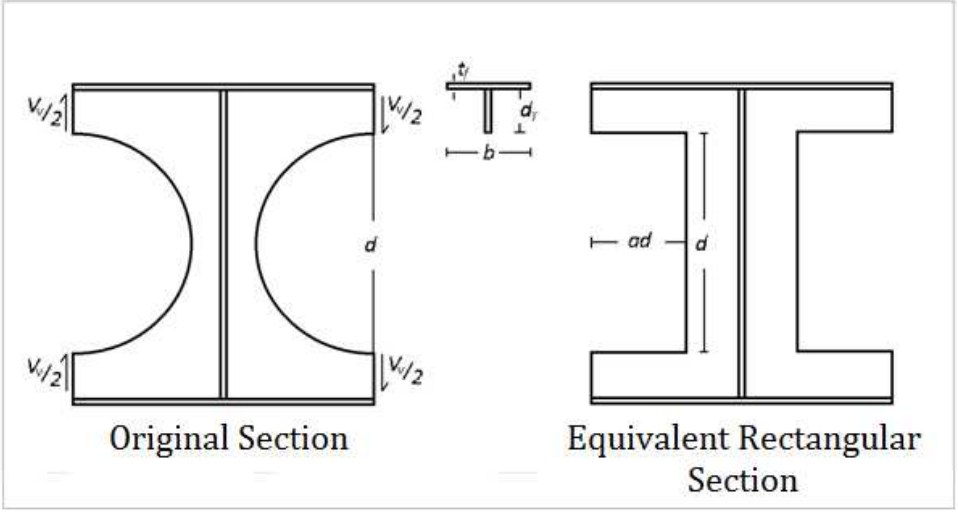

Figure 25: Illustration for the lower bound of the Vierendeel shear capacity. The original and its equivalent rectangular opening are shown.

To calculate the elastic moment capacity:

$$M_{elastic} = S_y p_y = \frac{I}{\bar{y}} p_y$$

Where I is the second moment of area of the tee section and $\bar{y}$ is the centroid.

The results are presented in **Table 11**.

S/d	1.1	1.1	1.1	1.2	1.2	1.2	1.3	1.3	1.3
t_w(mm)	5	7.6	10.5	5	7.6	10.5	5	7.6	10.5
σ(Mpa)	259	311	331	250	304.5	328	165	250	295

Table 11: Compressive stresses for the models studied, considering Vierendeel bending moment capacities.

These values accurately predict the failure mode of the stiffened models with spacing of openings at 1.1 and 1.2. However, for the spacing of the openings of 1.3, the failure mode is mostly governed by buckling actions due to a lack of utilisation of the stiffeners and a small S/d ratio. Therefore, the lower bound would be that of BS5950–1:2000. **Figure 26** presents the graphs of **Tables 9** and **11**:

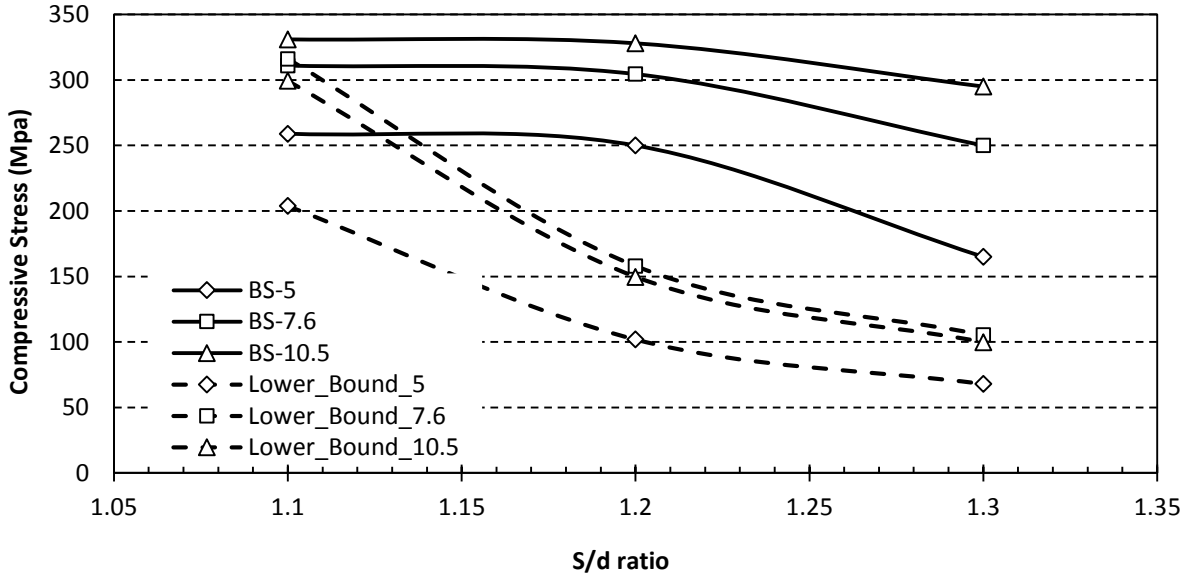

Figure 26: Evaluation of minimum compressive stresses from BS5950–1:2000(BS), and Vierendeel moment capacity (Lower_Bound).

t_w(mm), t_s(mm)	C_1	C_2	C_3
5, 5	1400	3570	2152
5, 10	450	1220	694.5
5, 15	1250	3165	1864
7.6, 5	750	2295	1504
7.6, 10	1250	3405	2096
7.6, 15	1250	3315	1965
10.5, 5	3500	9070	5592
10.5, 10	2100	5630	3476
10.5, 15	500	1670	1020

Table 12: Coefficients C_1, C_2 and C_3 of empirical design formula.

Consequently, for $S/d = 1.1, 1.2$ the Vierendeel moment capacity is critical for the design of perforated cellular beams with concentric transverse stiffeners. For $S/d = 1.3$, the BS5950–1 strut analogy for buckling is critical.

An empirical design equation has been developed, similar to the equation derived in the literature [5] from the results of **Figure 5** to **Figure 7**. This equation is as follows:

$$V_v = -C_1(S/d)^2 + C_2(S/d) - C_3$$

The coefficients for the design formula were found and are presented in **Table 12**.

5. Conclusions and Recommendations

A FE theoretical investigation was carried out using ANSYS concerning double concentric transversely stiffened cellular beams with closely spaced perforations. There were a total of 31 computations models. The parameters studied were the S/d ratio, the web thickness and the stiffener thickness.

Summarizing the results, it was found that the transverse stiffeners were very effective for $S/d < 1.3$, while for $S/d \geq 1.3$ they were almost ineffective; hence 1.3 was set as the upper limit. More research into the values between 1.2 and 1.3 could identify the point for designers at which the choice of stiffener remains an economic option. The models, as expected, appeared to have increased strength with increasing web thickness and stiffener thickness. Vierendeel shearing was the failure mode for the vast majority of models with $S/d < 1.3$ (17 out of 18), while at 1.3 the results were mixed with buckling appearing to be the dominating failure mode (6 out of 9).

Transverse stiffeners alter the position of plastic hinges. Whilst the unstiffened section formed plastic hinges near the flanges ($0.25d$), the stiffened sections formed plastic hinges closer to the mid height of the web-post ($0.45d$).

Stresses in the stiffeners started to develop at the height of the plastic hinges, expanding upwards and downwards. At failure, the top and bottom parts of the stiffeners remained unstressed, while the stresses that developed in the central area were of a comparatively lower magnitude for the majority of the results. Finite element method analyses show that by restricting placement of the stiffeners to only span the parts of the section that actually become stressed, the manufacture of transverse stiffeners would become easier (without the need for chamfering) and more economic.

By studying the failure patterns of the buckling imperfections predicted by ANSYS, three distinct patterns emerged: patterns A, B and C. The final failure deformations of the models appeared to be affected by these patterns and therefore applying horizontal eccentricity for sections with $S/d > 1.3$ could provide further avenues for experimental research.

Alternatively, a reasonable option could be to use a different type of stiffening for openings with $S/d > 1.3$. Ring stiffeners (hoops) around the edge of the openings could provide a suitable alternative as the strength of this type of stiffening does not seem to diminish with an increasing S/d. Theoretical investigations with rings have not been conducted. Research for this type of stiffener could provide information on how to effectively design for shear within the context of stiffened perforated beams with widely spaced perforations, despite the associated cost.

The variety of web opening shapes and sizes could also be considered in future research. The effects of transverse stiffeners or rings on elliptical and rectangular web openings found on previous research should be further studied.

Concerning the design model, for $S/d = 1.1, 1.2$ the Vierendeel moment check was chosen, and for $S/d = 1.3$ the BS5950 – 1 strut analogy check was selected.

At last, it is important to note that research on stiffeners with perforated beams, as well as on unstiffened perforated beams, is yet to be fully explored while the knowledge of their behaviour is limited. Detailed research should lead to update the existing available recommendations and replace them with design guidelines providing more construction options for engineers, leading to more economic, visually appealing, and efficient complex structures.

References:

[1] SCI (2014), *Steel Beams with Web Openings,* SCI. [online] available at: http://www.steel-insdag.org/.

[2] Fabsec Ltd. (2006), *Design of FABSEC Cellular Beams in Non-composite and Composite Applications for Both Normal Temperature and Fire Engineering Conditions*, Fabsec Limited.

[3] M. Feldmann (2006), *Large web openings for service integration in composite floors*, Contract No: RFS-CT-2005-00037.

[4] Chung, K.F, Liu, C.H. and Ko, A.C.H (2003), *Steel beams with large web openings of various shapes and sizes: An empirical design method using a generalised moment-shear interaction curve,* Journal of Constructional Steel Research, v 59, n 9, p 1177-1200.

[5] K.D. Tsavdaridis and C. D'Mello (2011), *Web buckling study of the behaviour and strength of perforated steel beams with different novel web opening shapes*, J Constr Steel Res, 67 (2011), pp. 1605–1620.

[6] K. D. Tsavdaridis, A.M.ASCE and C. D'Mello (2012), *Vierendeel Bending Study of Perforated Steel Beams with Various Novel Web Opening Shapes through Nonlinear Finite-Element Analyses,* J. Struct. Eng., 138(10), 1214–1230.

[7] KC Rockey, G Valtinatand KH Tang (1981), *The Design of Transverse Stiffeners on Webs Loaded in Shear – an Ultimate Load Approach*, Proceedings of the Institution of Civil Engineers, Vol. 71, Issue 4, Part 2, 1069-1099.

[8] Horne, M. R. and Grayson, W. R. (1983), *Parametric Finite Element Study of Transverse Stiffeners for Webs in Shear,* Instability and Plastic Collapse of Steel Structures, Proceedings of the Michael R. Horne Conference, L. J. Morris (ed.), Granada Publishing, London, 329 – 341.

[9] K. N. RAHAL and J. E. HARDING (1990), *Transversely stiffened girder webs subjected to shear loading – part 1: behaviour* , ICE Proceedings, Volume 89, Issue 1, 1990, pp. 47-65.

[10] K. N. RAHAL, J. E. HARDING and B. RICHMOND (1990), *Transversely stiffened girder webs subjected to shear loading – part 2: design,* ICE Proceedings, Volume 89, Issue 1, 1990, pp. 67 –87.

[11] K. N. RAHAL and J. E. HARDING (1991), *Transversely stiffened girder webs subjected to combined in-plane loading,* ICE Proceedings, Volume 91, Issue 2, 1991, pp. 237 –258.

[12] G S STANWAY, J C CHAPMAN and P J DOWLING (1993), *Behaviour of a web plate in shear with an intermediate stiffener,* Proceedings of the ICE - Structures and Buildings, Volume 99, Issue 3, 01 August 1993 , pages 327 –344.

[13] G S STANWAY, J C CHAPMAN and P J DOWLING (1996), *A design model for intermediate web stiffeners*, Proceedings of the ICE - Structures and Buildings, Volume 116, Issue 1, 01 February 1996 , pages 54 –68.

[14] Xie, M., Chapman and J. C. (2003), *Design of web stiffeners: Axial Forces,* J. Constr. Steel Res., 59_8_, 1035–1056.

[15] Xie, M., Chapman, and J.C., Hobbs, R.E. (2008), *A rational design model for transverse web stiffeners*, Journal of Constructional Steel Research, 64 (9), pp. 928-946. [16] J. C. Gibbons, N. R. Baddoo, A. W. Morrow and C. Gibbons (1999), *A comparison to Eurocode 3: Part 1.1 with BS5950 – 1: Part 1*, SCI 3rd Edition.

[17] J Rhodes, D Nash and M Macdonald, *Some aspects of Web Crushing Behaviour in Thin-Walled Beams' 8th Polish Symposium on Stability of Structures*, Sept 23-25 1997, Zakopane, Poland

[18] British Standards Institution, BS5950 – 1:2000, *Structural use of steelwork in buildings,* BSI; 2000.